International Research Journal of Innovations in Engineering and Technology (IRJIET)

ISSN (online): 2581-3048
Volume 6, Issue 10, pp 70-78, October-2022
https://doi.org/10.47001/IRJIET/2022.610011

Numerical Analysis of Flexural Behavior of Reinforced Concrete Beams Strengthened with Near Surface Mounted FRP Bars

[1]*Khadija Mohamed, [2]Ezz Eldin Mostafa, [3]Ayman Hussein

[1]*MSc Student, Department of Structural Engineering, Faculty of Engineering, Ain Shams University, Cairo, Egypt
[2]Assistant Professor, Department of Structural Engineering, Faculty of Engineering, Ain Shams University, Cairo, Egypt
[3]Professor of Concrete Structures, Department of Structural Engineering, Faculty of Engineering, Ain Shams University, Cairo, Egypt

***Abstract* - Recently, the near-surface-mounted (NSM) technique has become an attractive alternative to the externally bonded (EB) technique. Compared to the EB technique, the NSM technique is less exposed to external damage sources and provides a stronger bond between the FRP reinforcement and the surrounding concrete. A numerical investigation utilizing the non-linear finite element modeling (FEM) was performed using ANSYS®software to validate experimental results. Analytical models were conducted to simulate the flexural behavior of Reinforced Concrete (RC) beams strengthened with NSM FRP bars considering the FRP Cross-sectional area, end-anchoring of the CFRP bar, and strengthening by partially bonded systems with different unbonded lengths. It was found that the modeling approach could simulate the experimentally measured beams behavior at all stages of loading with an acceptable degree of accuracy.**

Keywords: Strengthening, FRP composite, NSM technique, CFRP reinforcement, Flexural strengthening capacity, Finite element modeling.

I. INTRODUCTION

Strengthening of reinforced concrete (RC) structures is one of the most important challenges in civil engineering. Deterioration of RC may occur due to destructive environmental conditions or internal material factors such as reinforcement corrosion, and poor concrete Production quality. Recently, the use of advanced composite materials (FRPs) for the strengthening of deteriorated structures has been embraced worldwide. Fiber-reinforced polymers (FRPs) were used instead of conventional concrete and steel due to their high strength-to-weight ratios, high corrosion resistance, high durability properties, and versatility of fabrication.

NSM strengthening technique is the use of FRP reinforcement embedded into grooves in the tension side of the strengthened elements. The NSM FRP reinforcement is bonded to the sides of the groove using epoxy adhesive or cementitious grout, where the grout fills all the empty spaces in the groove. Then, the groove is filled and the surface is leveled, as shown in Figure 1. The NSM technique is less exposed to environmental and damage sources Compared to the EB technique. Also, it provides a stronger bond to the surrounding substrate rather than the EB technique and increases both flexural and shears strength. However, one of the most common failure modes of RC beams strengthened with the NSM technique is debonding by concrete cover separation, which initiates and completes at relatively low strain levels in the FRP element [1]–[7].

Compared to the EB FRPs, the NSM technique does not require any surface preparation and it can be anchored into the adjacent concrete members. Furthermore, NSM FRP reinforcing systems show higher bond strength when compared to EB FRP systems because of their larger bond stress transfer area and being confined by the surrounding concrete. Moreover, contrary to the EBR, the NSM reinforcements can attain high values of tensile stress. Furthermore, the NSM technique is even more attractive in negative moment regions than in positive moment regions as it is less exposed to fire, accidental impact, and vandalism [7]–[9].

(a) **(b)**

Figure 1: Near-surface mounted (NSM) FRP strengthening technique

II. PREVIOUS EXPERIMENTAL DATA

In 2018, Islam[10]Tested six RC beams with a rectangular section of 150×250 mm^2 and a total length of 2500 mm to study their flexural behavior. The six beams were

International Research Journal of Innovations in Engineering and Technology (IRJIET)

ISSN (online): 2581-3048

Volume 6, Issue 10, pp 70-78, October-2022

https://doi.org/10.47001/IRJIET/2022.610011

tested under 4-point loading with 2250 mm clear flexural span and 775 mm shear span up to failure. The load was applied using a 1000 kN capacity servo-controlled hydraulic jack (ENERCAP), and monitored using a 1000 kN capacity load cell. A stiffened steel spreader (HSB-160) was attached to the hydraulic ram to divide the single point load transferred from the jack into two equal concentrated loads as shown in Figure 2.A control beam (CB) was tested without being strengthened, whereas the other five beams were strengthened with NSM CFRP deformed bars.

Figure 2: Test specimen details of CB

For the CB, the tension and compression reinforcement were 2-M10deformed steel bars. The section of the CB was under-reinforced with a ratio of bottom steel reinforcement (ρ = 0.0042). The beam was designed to avoid compression failure due to concrete crushing according to ACI 440.2R-08 [11] specifications. The shear reinforcement consisted of 8 mm diameter smooth steel stirrups, uniformly spaced at 100 mm center to center. The concrete clear cover (measured from the stirrup centerline to the concrete surface) for the tension and compression steel reinforcement was 34 and 24 mm, respectively. Figure shows the geometry and reinforcement details of the CB.

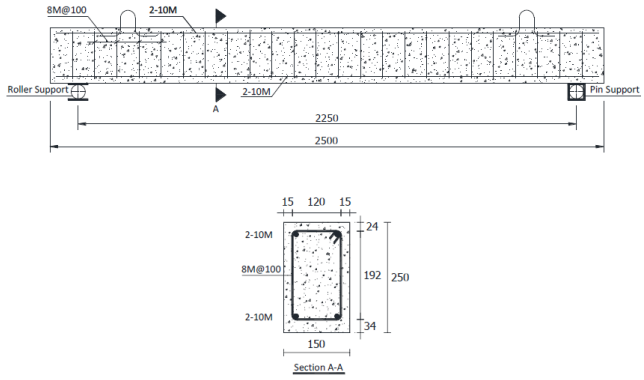

Figure 3: Test specimen details of CB[10]

For the other five beams (S1F, S2F, A2F, A2P35, and A2P45), the ordinary reinforcement was as the CB while they were strengthened with NSM CFRP bars with a 10 mm nominal diameter and a 2000 mm limited length. The CFRP bars were manufactured with two different end conditions (i.e. straight and hooked). The hooked end was manufactured with a 100 mm length. The main purpose of using the hooked ends is to act as an anchorage system to delay or prevent the concrete cover separation. Beam S1F was strengthened with one fully bonded-straight bar. Beam S2F was strengthened with two fully bonded straight bars. Beam A2F was strengthened with two fully bonded end-anchored bars. Beams A2P35 and A2P45 were strengthened with two partially bonded end-anchored bars, having different unbounded lengths. For the beam, A2P35, the unbonded length was selected to be 70 times the bar diameter, running along the constant moment region. While for beam A2P45, the unbonded length was extended into the shear span zone to be 90 times the bar diameter. A test matrix summary of the tested beams is shown in Table 1. Figure4 shows the strengthening scheme for the five beams.

Table 1: Test Matrix

Beam ID	Number of CFRP bars N_b	End Condition	Unbonded length L_{ub}, mm	Test variable
CB	------	------	------	CB
S1F	1	Straight End	Fully Bonded	NSM Area
S2F	2	Straight End	Fully Bonded	NSM Area
A2F	2	Hooked End	Fully Bonded	Anchorage System
A2P35	2	Hooked End	70 d_b	Partial bonding + unbonded Length
A2P45	2	Hooked End	90 d_b	Partial bonding + unbonded Length

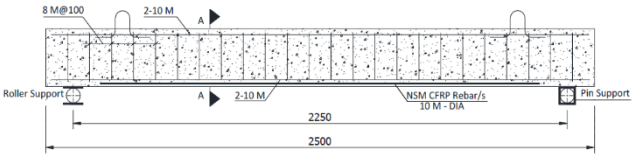

(a) Side view of beams S1F and S2F

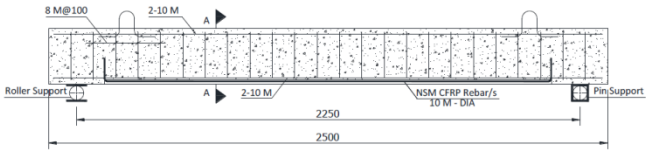

(b) Side view of beams A2F and A2P35, and A2P45

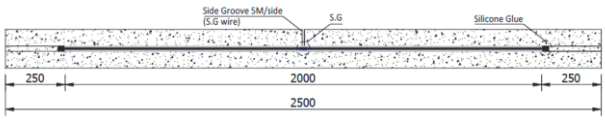

(c) Bottom view of beams S1F

International Research Journal of Innovations in Engineering and Technology (IRJIET)

ISSN (online): 2581-3048

Volume 6, Issue 10, pp 70-78, October-2022

https://doi.org/10.47001/IRJIET/2022.610011

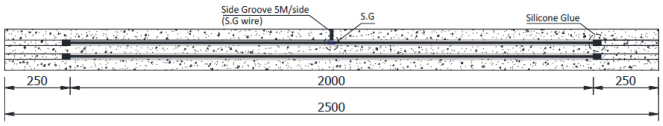

(d) Bottom view of beams S2F and A2F

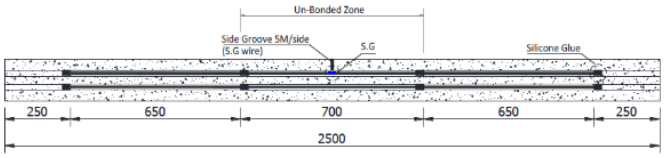

(e) Bottom view of beam A2P35

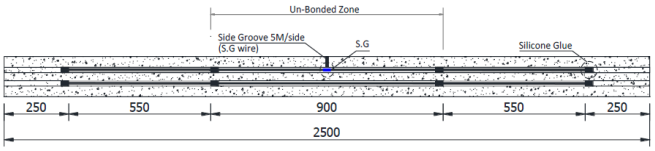

(f) Bottom view of beam A2P45

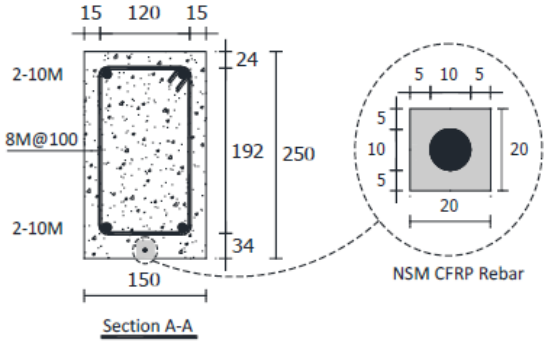

(g) Cross section of beam S1F

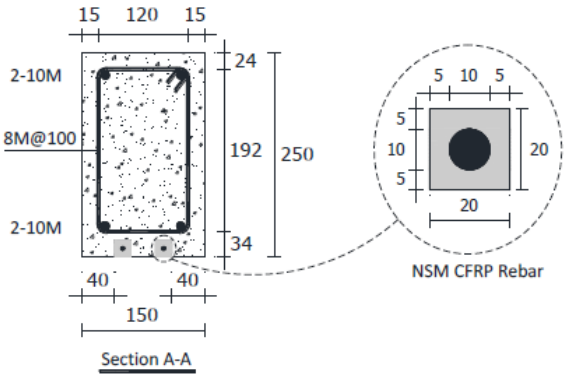

(h) Cross section of beams S2F, A2F, A2P35, and A2P45

Figure 4: Beams strengthening schemes [10]

III. FINITE ELEMENT ANALYSIS

To simulate the behavior of RC beams strengthened with NSM CFRP bars, ANSYS software[12] is used. It is consideredOne of the most powerful non-linear finite element software, and it was chosen in this present work because of its popularity and capabilities in the plasticity analysis of concrete. It can be utilized in the prediction of concrete behavior in the pre-and post-cracking stages, and the behavior of reinforcement before and beyond yielding.

The FE models were conducted using the commercial software ANSYS®-version 15. Only one-quarter of each specimen was modeled to save computational time. The direct mesh generation was chosen to completely control the model; however, it consumes much more time compared to the solid modeling technique. The adequate element type and material constitutive model were carefully selected to simulate the behavior of concrete, steel reinforcement bars, CFRP, and epoxy adhesive.

3.1 Element Types

SOLID65 (Eight-node solid brick element) was used to model the geometric discretization of concrete and filling material (epoxy adhesive). SOLID65 is a three-dimensional isoparametric element. This element has eight nodal points with three degrees of freedom for each node. These nodes have translations in the nodal x, y, and z directions, without rotations. Figure shows the element geometry, the coordinate system, and the locations of its nodes.

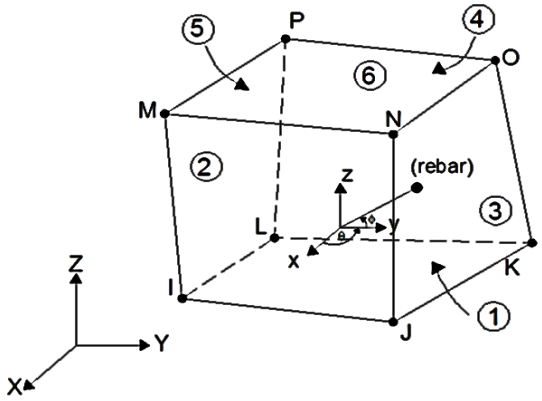

Figure 5: SOLID65 Element Geometry [12]

SOLID185 (Eight-node solid brick element) was used to model the loading and supporting apparatus because of the stress concentration problem, which leads to the localized crushing of concrete elements near the loading and bearing areas. Steel plates are modeled by SOLID185 at the location of loading and support locations in the studied strengthened beams. Moreover, it provides uniform stress distribution at supports and loading locations. This element is defined by eight nodes having three degrees of freedom at each node, translations in the global x, y, and z directions. Figure shows the element geometry, the locations of its nodes, and the coordinate system.

International Research Journal of Innovations in Engineering and Technology (IRJIET)

ISSN (online): 2581-3048

Volume 6, Issue 10, pp 70-78, October-2022

https://doi.org/10.47001/IRJIET/2022.610011

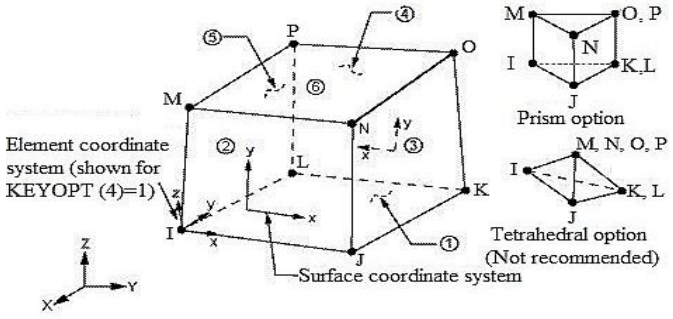

Figure 6: SOLID 185 Element Geometry [12]

LINK180 (2-Node structural bar element) was used to model the steel reinforcement and CFRP bars. As shown in Figure 7, it is a 2-node bar linear element. Each node has three degrees of freedom, translations in the nodal x, y, and z directions. The element is a uniaxial tension-compression element. The axial stress is assumed to be uniform over the entire element.

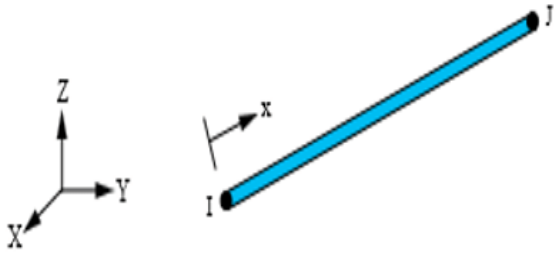

Figure 7: LINK180 Element Geometry [12]

3.2 Concrete Material Modeling

3.2.1 Stress-Strain Curve of Concrete in Compression

The non-linear plastic behavior of concrete under uniaxial compression was obtained from the Hognestad [13] model. Figure 8 shows the Hognestad-Popvics stress-strain curve which were used for the representation of the concrete model in compression. The stress-strain model can be presented in the following equations:

$$f_C = f'_C\left[\left(\frac{2\varepsilon_c}{\varepsilon_0}\right) - \left(\frac{\varepsilon_c}{\varepsilon_0}\right)^2\right] \quad for\ 0 \le \varepsilon_c \le \varepsilon_0 \qquad \text{Eq. 1}$$

$$f_C = f'_C - \frac{0.15\, f'_C}{(\varepsilon_{cu} - \varepsilon_{c0})} \quad for\ 0 \le \varepsilon_c \le \varepsilon_0\ , \varepsilon_0 = \frac{2f_C}{E_c} \qquad \text{Eq. 2}$$

Where

f_C : is the compressive stress at any strain (ε_c);

f'_C and ε_0 : are the maximum compressive stress and its corresponding strain;

ε_{cu} and f_u : are the ultimate strain and its corresponding stress, which are assumed to be 0.003 and 0.85f'c, respectively;

E_c: is the initial Young's modulus of concrete, and is defined according to ACI 318-18 (440,2003) by the following equation:

$$E_c = 4700\sqrt{f'_c} \qquad \text{Eq. 3}$$

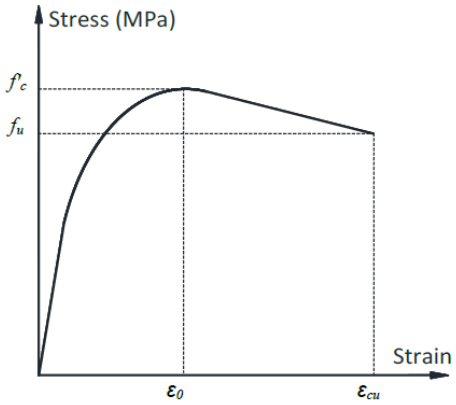

Figure 8: Concrete constitutive models for compression [13]

3.2.2 Stress-Strain Curve for Concrete in Tension and Shear

The stress-strain curve for concrete in tension is shown in Figure 9. The ability of cracked concrete to pick up tensile stresses between cracks is modelled through tension softening in ANSYS®. After reaching the rapture strength of concrete (f_t), the tension softening is represented by a 40% sudden drop in the tensile stress, followed by a gradual decline to reach zero stress at a ($6\varepsilon_t$) strain, where ε_t is the tensile strain corresponding to f_t. The rapture strength (f_t) of concrete was adopted as $0.56\sqrt{f'_c}$[11].

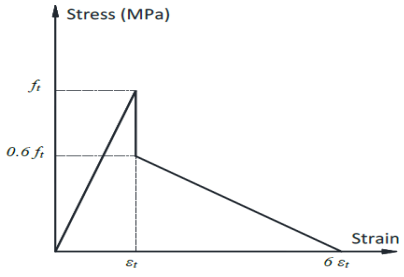

Figure 9: Concrete constitutive models for tension

The shear transfer factor is introduced for smeared modeling of aggregate interlock and dowel bar shear resisting mechanisms in cracked concrete. The shear transfer (βt) coefficient typically ranges from 0.0 to 1.0 [12], in which 0.0 implies complete loss of shear transfer (very smooth crack) and 1.0 implies loss of shear transfer (very rough crack). In the current study, the shear strength reduction factor for cracked concrete is applied for both the open and closed shear transfer coefficients. The open shear transfer coefficient is taken as 0.2 and the closed shear transfer coefficient was taken as 0.2.

International Research Journal of Innovations in Engineering and Technology (IRJIET)

ISSN (online): 2581-3048

Volume 6, Issue 10, pp 70-78, October-2022

https://doi.org/10.47001/IRJIET/2022.610011

3.3 Steel Reinforcement and Steel Plates Modeling

The steel reinforcement was assumed to have an elastic-perfectly plastic non-linear response with a poison's ratio of 0.30 for all types of steel reinforcement. The Von-Mises criterion was employed to define the yielding phenomenon.

The steel loading and supporting apparatus were assumed to have a linear elastic material with a modulus of elasticity and Poisson's ratio of 200 GPa and 0.30. Figure shows the stress-strain curve assigned to steel reinforcement and steel plates.

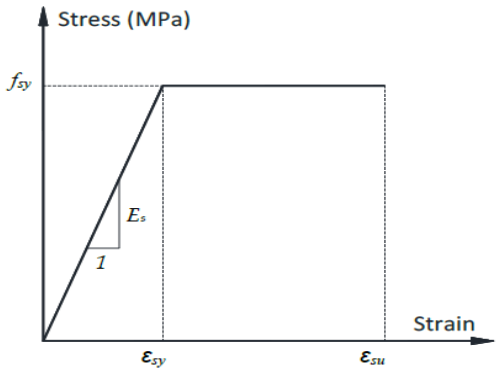

Figure 10: steel constitutive material model

3.4 CFRP bar and Epoxy adhesive

The CFRP material was considered to be linear elastic isotropic with a Poisson's ratio of 0.35. The stress-strain curve of the FRP bars is shown in Figure 11. A multi-linear elastoplastic diagram was used to define the behavior of the epoxy adhesive along with the same concrete cracking model without considering the tension softening phenomenon. The Poisson's ratio was taken as 0.37 for the epoxy adhesive. The schematic stress-strain curve of the epoxy adhesive is shown in Figure 12.

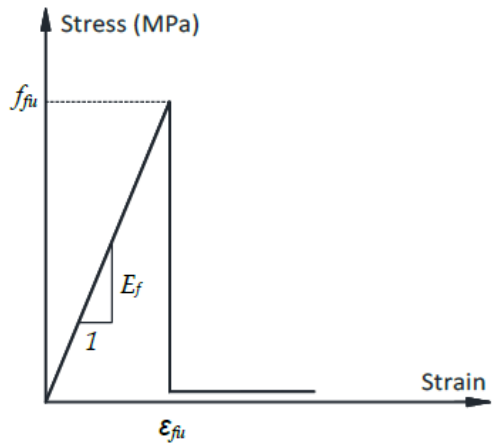

Figure 11: Stress-strain curves for CFRP bar

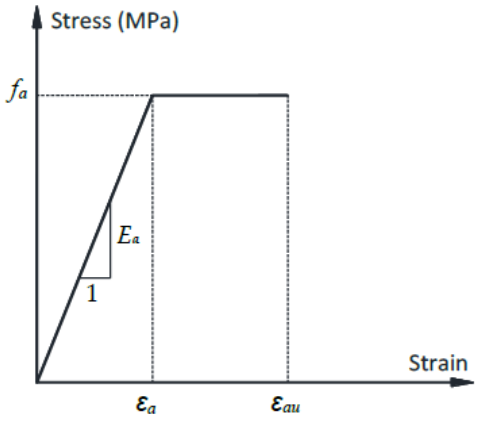

Figure 12: Stress-strain curves for Epoxy adhesive

3.5 Modeling of CFRP bar-Epoxy interaction

To simulate the bond-slip behavior at the CFRP bar-epoxy interface, the spring damper (COMBIN14) was employed. The damping capability of COMBIN14 was removed by assigning zero values to the damping coefficients. The spring stiffness was calculated using Eq. 4 [14]. It should be noted that no pullout tests were conducted in this research, therefore, values of the maximum bond stress and its corresponding strain were properly assumed.

$$k = \frac{\pi}{s_u} \mathrm{P}\, d_b\, \mathrm{n}\, \Gamma_{bu} \left(\frac{L_1 + L_2}{2}\right) \qquad \text{Eq.4}$$

Where s_u is the slip value corresponding to the maximum bond stress (Γ_{bu}), p is the horizontal distance between bars, d_b is the bar diameter, n is the number of bars, and L_1 and L_2 are the lengths of two adjacent LINK180 (FRP) elements.

3.6 Modeling of Epoxy–Concrete interface

To analyze the epoxy-concrete interface debonding, a particular continuum damage approach, called the cohesive zone model (CZM), along with the fracture mechanics were used. The CZM model assumes that the stress transfer between the separate faces is not completely lost at debonding initiation, but rather is a gradual stiffness reduction of the interface between them. In such a model, fracture mechanics failure criteria are used to detect debonding initiation, and debonding evolution is predicted in terms of softening relationships between tractions and the separations. Both, the contact elements with zero thickness and interface elements with finite thickness can use the CZM traction-separation constitutive model in ANSYS®[15]. In this research, the perfect bond was assumed at the vertical epoxy-concrete interface of the end hooks. The perfect bond requires merging the concurrent nodes for the whole model in ANSYS®, which is not recommended when using the contact elements.

International Research Journal of Innovations in Engineering and Technology (IRJIET)

ISSN (online): 2581-3048

Volume 6, Issue 10, pp 70-78, October-2022

https://doi.org/10.47001/IRJIET/2022.610011

Therefore, contact elements were used for the FE models of the non-anchored NSM systems (without end hooks), while the interface elements were used for the FE models of the anchored NSM systems (with end hooks). The geometry of the contact and interface elements is shown in Figure and Figure , respectively.

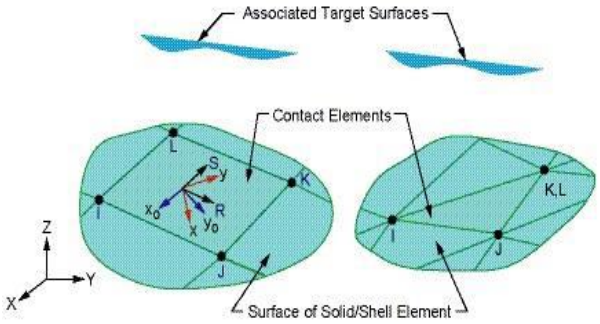

(a) Geometry of CONTA173

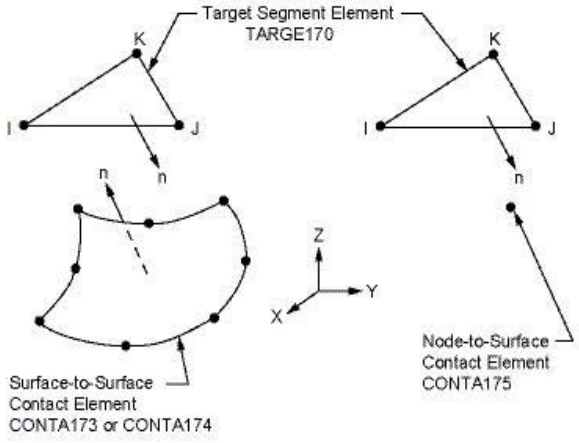

(b) Geometry of TARGE170

Figure 13: Geometry of the contact pair elements

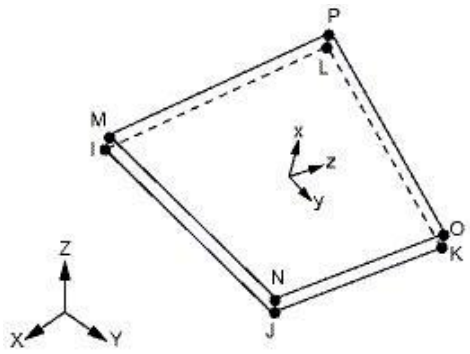

Figure 14: Geometry of INTER205 element

3.7 Meshing of Finite Element Model

The accuracy of finite element relies on selection of the suitable mesh shape and divisions. The FE models were conducted with refined mesh applied at the locally high stressed zones.

Figure Figure 15 shows the used mesh in the developed models. Two mesh sizes were used: 12.5 mm for the entire structure except the first 100 mm before the CFRP bar end and inside the NSM groove; the mesh size was reduced to 2.5 mm at these locations.

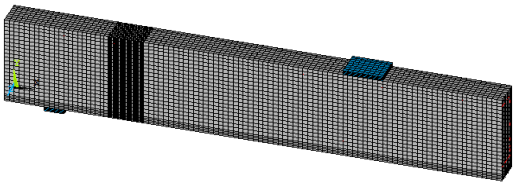

Figure 15: Mesh of the developed FE models

3.8 Non-linear analysis and Convergence Criteria

Different control techniques have been devised to perform non-linear analysis. These techniques are force control, displacement control. In this study, the non-linear solution was operated using a force control mode with a 10 N load increment. In contrast to displacement control mode, the force control mode consumes a little time in solving such complex models; however, it cannot track the post-peak behaviour of the modeled specimen.

Due to the non-linear behaviour of concrete, it was difficult to achieve the solution convergence for the developed models. Therefore, the force convergence tolerance limit was increased from 0.005 (the default tolerance limit defined in ANSYS®) to 0.10. The Newton-Raphson equilibrium iterations were used to update the global stiffness matrix after the completion of each load increment.

IV. VERIFICATION OF ANALYTICAL MODELS WITH EXPERIMENTAL RESULTS

To have a reliable numerical model, the six tested beams (CB, S1F, S2F, A2F, A2P35, and A2P45) were developed in ANSYS software[12]. As shown in Figure 16, good agreement is noticed between the experimental and analytical crack patterns for each beam. Figure 17 compares the numerical and experimental (P-Δ) curves. The comparison indicates that there is a good correlation between the FE and experimentally obtained results. Table presents the comparison details for the cracking load, yielding load, ultimate load, and their corresponding deflection.

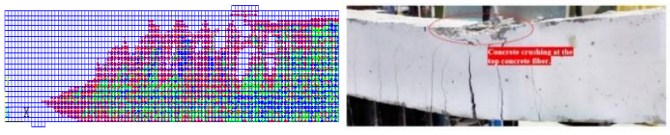

(a) Control beam (CB)

International Research Journal of Innovations in Engineering and Technology (IRJIET)

ISSN (online): 2581-3048

Volume 6, Issue 10, pp 70-78, October-2022

https://doi.org/10.47001/IRJIET/2022.610011

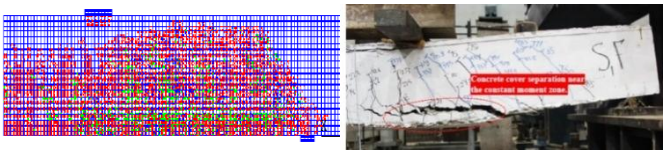

(b) Beam S1F

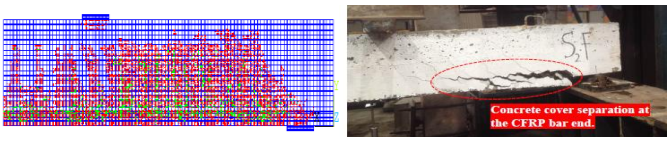

(c) Beam S2F

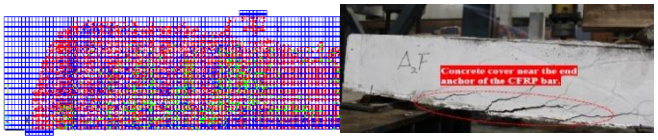

(d) Beam A2F

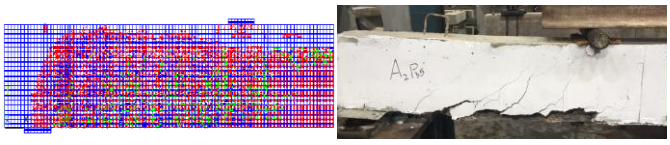

(e) Beam A2P35

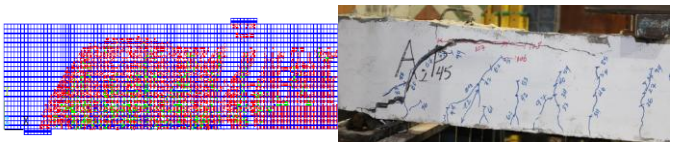

(f) Beam A2P45

Figure 16: Predicted and Observed Cracking Patterns for Specimens

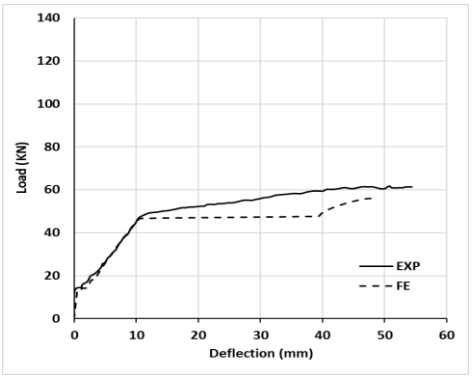

(a) Control Beam (CB)

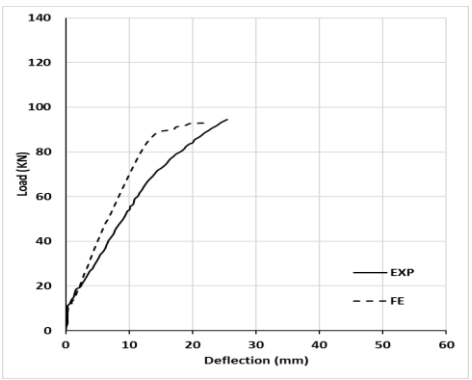

(b) Beam S1F

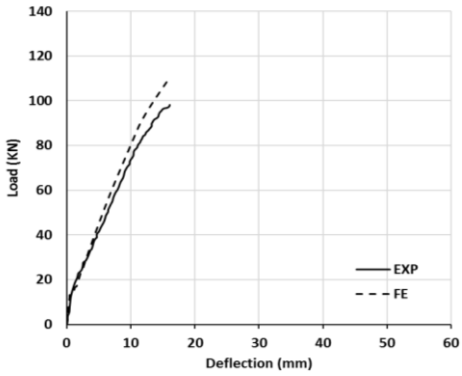

(c) Beam S2F

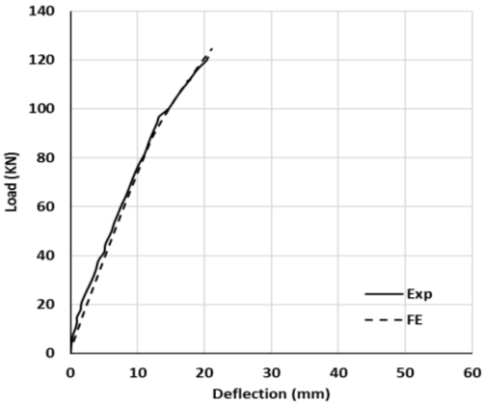

(d) Beam A2F

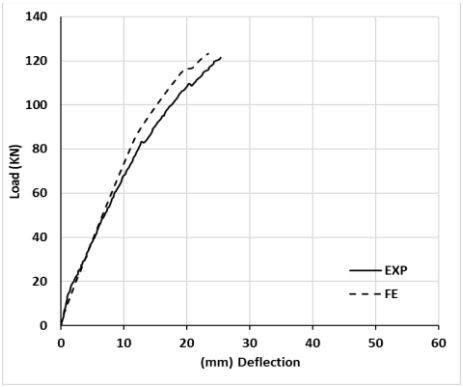

(e) Beam A2P35

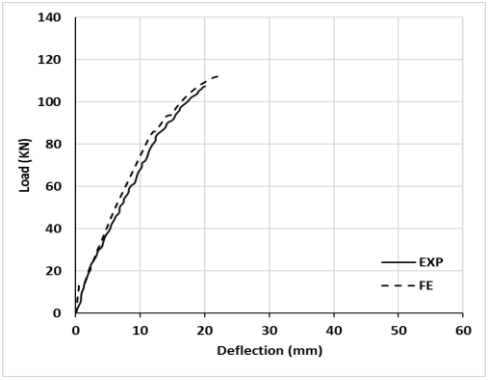

(f) Beam A2P45

Figure17: Comparison between experimental and numerical load-deflection curves

ISSN (online): 2581-3048
Volume 6, Issue 10, pp 70-78, October-2022
https://doi.org/10.47001/IRJIET/2022.610011

Table 2: Key points of load-deflection curves; Comparison of test results obtained by (Islam Shokry, 2018) with FE results

Beam ID	Results	P_{cr}, KN	Δ_{cr}, mm	P_y, KN	Δ_y, mm	P_u, KN	Δ_u, mm
CB	Exp.	15	1.2	47	10.3	61.3	58.3
	FE	13.8	1.24	45.8	10.3	57	49
	Error (%)	-8	3.3	-2.5	0	-7	-15.9
S1F	Exp.	15.1	1.5	64	12.7	96	28
	FE	13.2	1.3	70	13.1	89.2	23
	Error (%)	-12.5	-13.3	9.3	3.1	-7	-17.8
S2F	Exp.	16.8	1.1	----	----	96.4	15.6
	FE	15	1	----	----	108	15.6
	Error (%)	-10.7	-9	----	----	12	0
A2F	Exp.	16.6	1.3	96	13.8	121.3	20.8
	FE	14.3	1.2	88	12.1	124.5	21.1
	Error (%)	-13.8	-7.7	-8.3	-12.3	2.6	1.4
A2P35	Exp.	17	1.7	84	13.6	120.5	25.3
	FE	16	1.5	84	12	123.2	23.5
	Error (%)	-5.8	-11.7	0	-11.7	2.3	-7.1
A2P45	Exp.	17	1.5	82	12.2	108	20.2
	FE	15	1.3	86	12.2	112	22
	Error (%)	-11.7	-13.3	4.87	0	3.7	8.9

V. SUMMARY AND CONCLUSIONS

This study introduces a simple realistic approach to simulate the flexural behavior of strengthened RC beams with NSM CFRP with different parameters using ANSYS software. The parameters comprised the FRP Cross-sectional area, end-anchoring of the CFRP bar, and strengthening by partially bonded systems with different unbonded lengths. Based on analytical and experimentally measured results of the studied beams, it is found that:

- The FEM model is considered reliable and could be used efficiently to investigate the flexural behavior of the strengthened beams with NSM CRFP bars with acceptable accuracy.

REFERENCES

[1] L. De Lorenzis and A. Nanni, "Strengthening of RC structures with near-surface mounted FRP rods," *Report*, vol. 1999, no. 3, pp. 565–575, 2002.

[2] T. Hassan and S. Rizkalla, "Investigation of Bond in Concrete Structures Strengthened with Near Surface Mounted Carbon Fiber Reinforced Polymer Strips," *J. Compos. Constr.*, vol. 7, no. 3, pp. 248–257, 2003, doi: 10.1061/(asce)1090-0268(2003)7:3(248).

[3] B. Täljsten, A. Carolin, and H. Nordin, "Concrete structures strengthened with near surface mounted reinforcement of CFRP," *Adv. Struct. Eng.*, vol. 6, no. 3, pp. 201–213, 2003, doi: 10.1260/136943303322419223.

[4] T. K. Hassan and S. H. Rizkalla, "Bond mechanism of near-surface-mounted fiber-reinforced polymer bars for flexural strengthening of concrete structures," *ACI Struct. J.*, vol. 101, no. 6, pp. 830–839, 2004, doi: 10.14359/13458.

[5] A. S. Kalayci, B. Yalim, and A. Mirmiran, "Construction tolerances and design parameters for NSM FRP reinforcement in concrete beams," *Constr. Build. Mater.*, vol. 24, no. 10, pp. 1821–1829, 2010, doi: 10.1016/j.conbuildmat.2010.04.022.

[6] F. Al-Mahmoud, A. Castel, R. François, and C. Tourneur, "RC beams strengthened with NSM CFRP rods and modeling of peeling-off failure," *Compos. Struct.*, vol. 92, no. 8, pp. 1920–1930, 2010, doi: 10.1016/j.compstruct.2010.01.002.

[7] R. El-Hacha and S. H. Rizkalla, "Near-Surface-Mounted Fiber-Reinforced Polymer Reinforcements for Flexural Strengthening of Concrete Structures," *ACI Struct. J.*, vol. 101, no. 5, pp. 717–726, Sep. 2004, doi: 10.14359/13394.

[8] L. De Lorenzis and A. Nanni, "Shear strengthening of reinforced concrete beams with near-surface mounted fiber-reinforced polymer rods," *ACI Struct. J.*, vol. 98, no. 1, pp. 60–68, 2001, doi: 10.14359/10147.

[9] D. H. Lim, "Flexural Behavior of Concrete Structures Strengthened With Nsm and Eb Cfrp Strips," *Engineering*, pp. 639–645, 2008.

[10] B. Islam Shokry Mohamed Aly Shabana, "FLEXURAL BEHAVIOUR OF RC BEAMS STRENGTHENED BY NEAR SURFACE MOUNTED FRP BARS," 2018.

[11] A. C. 440, "ACI 440.1R-03. Guide for the design and construction of concrete reinforced with FRP bars," *Am. Concr. Inst. (ACI), Farmingt. Hills, Mich., USA*, p. 42pp, 2003.

[12] ANSYS, *No Title*. ANSYS Mechanical, v15, Help system, 18.2 ed., 2015.

[13] E. Hognestad, N. W. Hanson, and D. McHenry, "Concrete Stress Distribution in Ultimate Strength Design," *ACI J. Proc.*, vol. 52, no. 12, pp. 455–480, Dec. 1955, doi: 10.14359/11609.

[14] J. Nie, J. Fan, and C. S. Cai, "Stiffness and Deflection of Steel–Concrete Composite Beams under Negative Bending," *J. Struct. Eng.*, vol. 130, no. 11, pp. 1842–1851, Nov. 2004, doi: 10.1061/(asce)0733-9445(2004)130:11(1842).

[15] Barbero, E.J., "Finite Element Analysis of Composite Materials Using ANSYS® - 2nd Edi." https://www.routledge.com/Finite-Element-Analysis-of-Composite-Materials-Using-ANSYS/Barbero/p/book/9781466516892 (accessed Jun. 06, 2021).

[16] CEB-FIP, "CEB Bulletins : CEB-FIP Model Code 90 (PDF)." https://www.fib-international.org/publications/ceb-bulletins/ceb-fip-model-code-90-pdf-detail.html (accessed Jun. 07, 2021).

[17] R. A. Hawileh, "Nonlinear finite element modeling of RC beams strengthened with NSM FRP rods," *Constr. Build. Mater.*, vol. 27, no. 1, pp. 461–471, 2012, doi: 10.1016/j.conbuildmat.2011.07.018.

[18] L. De Lorenzis and J. G. Teng, "Near-surface mounted FRP reinforcement: An emerging technique for strengthening structures," *Compos. Part B Eng.*, vol. 38, no. 2, pp. 119–143, 2007, doi: 10.1016/j.compositesb.2006.08.003.

[19] H. Y. Omran and R. El-Hacha, "Nonlinear 3D finite element modeling of RC beams strengthened with prestressed NSM-CFRP strips," *Constr. Build. Mater.*, vol. 31, pp. 74–85, 2012, doi: 10.1016/j.conbuildmat.2011.12.054.

ISSN (online): 2581-3048
Volume 6, Issue 10, pp 70-78, October-2022
https://doi.org/10.47001/IRJIET/2022.610011

AUTHORS BIOGRAPHY

Khadija Mohamed is an MSc student at the Department of Structural Engineering, Faculty of Engineering, Ain Shams University, Cairo, Egypt. khadijaelbadawy16@gmail.com

Ezz El-Deen Mostafa is an Assistant Professor at the Department of Structural Engineering, Faculty of Engineering, Ain Shams University, Cairo, Egypt. ezzeldin.mostafa@eng.asu.edu.eg

Aymen Hussein is a Professor of Concrete Structures at the Department of Structural Engineering, Faculty of Engineering, Ain Shams University, Cairo, Egypt. ayman.hussein.khalil@eng.asu.edu.eg

Citation of this Article:

Khadija Mohamed, Ezz Eldin Mostafa, Ayman Hussein, "Numerical Analysis of Flexural Behavior of Reinforced Concrete Beams Strengthened with Near Surface Mounted FRP Bars" Published in *International Research Journal of Innovations in Engineering and Technology - IRJIET*, Volume 6, Issue 10, pp 70-78, October 2022. Article DOI https://doi.org/10.47001/IRJIET/2022.610011

****

